BJRS

BRAZILIAN JOURNAL
OF
RADIATION SCIENCES
08-03A (2020) 01-14

Crystallographic texture of hot rolled uranium-molybdenum alloys

Nielsen[a,b] G.F., Morais[b] N.W.S., Lima[b] N.B.

[a] *Centro Industrial Nuclear de Aramar/Departamento de Materiais Nucleares, 18560-000, Iperó, SP, Brazil*

[b] *Instituto de Pesquisas Energéticas e Nucleares, 05508-000, São Paulo, SP, Brazil*

guilherme.nielsen@marinha.mil.br

ABSTRACT

The uranium molybdenum (U-Mo) alloys have the potential to be used as low enriched uranium nuclear fuel in research, test, and power nuclear reactors. U-Mo alloy with composition between 7 and 10 wt% molybdenum shows excellent body centered cubic phase (γ phase) stabilization and presents a good nuclear fuel testing performance. Hot rolling is commonly utilized to produce nuclear fuel plate where it promotes the cladding and the fuel alloy bonding. The mechanical deformation generates crystallographic preferential orientation, the texture, which influences the material properties. This work studied the texture evolution in hot rolled U-Mo alloys. The U7.4Mo and U9.5Mo alloys were melted in a vacuum induction furnace, homogenized at 1000°C for 5 h, and then hot rolled at 650°C in three height reductions: 50, 65 and 80%. The crystalline phases and the texture were evaluated by X-ray diffraction (XRD). The as-cast and processed alloys microstructures were characterized by optical and electronic microscopies. The as-cast, homogenized, and deformed alloys have the γ phase. It was found microstructural differences between the U7.4Mo and U9.5Mo alloys. The homogenized treatment showed effective for microsegregation reduction and was not observed substantial grain size increasing. The deformed uranium molybdenum alloys presented α, γ, θ texture fibers. The intensity of these texture fibers changes with rolling reduction.

Keywords: **U-Mo alloys, hot rolling, texture.**

ISSN: 2319-0612
Accepted: 2020-08-18

1. INTRODUCTION

The Reduced Enrichment Program for Research and Test Reactors (RERTR) was initiated in 1978 to develop technology to convert and operate nuclear reactors with low uranium enrichment nuclear fuels [1,2]. This program limited the enrichment of nuclear fuel production up to 20% by weight of the fissile isotope ^{235}U, called Low Enriched Uranium (LEU). Monolithic fuels are employed to increase the density of fissile material in nuclear fuels. These fuels are usually produced in the form of plates where their core is the fissile material and its cladding by zirconium or stainless steel. These fuels have high thermal conductivity and an intermediate melting point. This high content of fissile material in thick plates, however, is undesirable because it causes excessive swelling [1,3].

Pure uranium has an orthorhombic uranium crystal system (α-U) at room temperature. This crystalline phase has some disadvantages such as high chemical reactivity (low oxidation resistance and high pyrophoricity), the anisotropy of properties, and swelling by irradiation [3]. To obtain better nuclear fuel performance, the metastable body centered cubic, bcc, (γ phase) of uranium should be achieved. Alloying elements are added to stabilize the uranium gamma phase [4]. The uranium-molybdenum alloys are one of the most commonly used monolithic fuels. This alloy from 7 weight percent (wt.%) of molybdenum stabilizes γ-uranium [1,5]. U10Mo was selected as a candidate with the best performance characteristics.

The rolling technique is the most employed for the production of nuclear fuel plates, [1,6,7]. The hot rolling process is normally used because it favors the fuel core and cladding bonding. Deformation processes modify the material microstructure and generate the preferential crystallographic orientation, the texture.

The understanding of the evolution of the microstructure and the mechanical properties during hot rolling is therefore essential to predict the behavior of the alloy under operational conditions and their damage by irradiation [8].

This work will evaluate the texture behavior under different hot rolling deformation conditions in the U7.4Mo and U9.5Mo (wt.%) alloys.

2. MATERIALS AND METHODS

The alloys were melted in the vacuum induction furnace. The as-cast alloys were submitted to a heat treatment to homogenize and stabilize the gamma phase at room temperature. The samples were heated for 5 hours at 1000°C followed by water quenching. The hot rolling temperature was 650°C. It was obtained for each alloy three samples with different deformations degree: 50, 65, and 80% of its initial thickness. The total rolling passes in 50, 65 and 80% deformed alloys were 5, 6, and 7, respectively.

Samples were generally cut by metallographic cutters using SiC abrasive discs. The samples were ground with 1200 mesh SiC paper. After grinding, the samples were polished using a 9 μm, 3 μm, and 1 μm diamond suspension. The electrolytic etching was performed with a solution of 6 parts of 10% H_2CrO_4 solution and 1 part of 10% HNO_3.

Chemical composition was obtained by Induced Coupled Plasma Optical Emission Spectroscopy (ICPOES) except carbon that was determined by the combustion method. To obtain reliable chemical composition results, the chemical analysis was performed in 6 g of material collected in several parts of the as-cast samples. The chemical composition results were presented from an average of 3 analyses. The optical and electronic microscopies were employed in the as-cast and homogenized samples.

The crystalline phase and texture were evaluated by x-ray diffractometry with Cu kα radiation. Rietveld refinement was accomplished using GSAS software [9]. The (110), (200), (211), and (310) pole figures were measured for the orientation distribution function (ODF) determination. The ODF calculation was made by MTEX software [10]. The ODF's were presented in Euler space as plots of 45° φ_2 section and its intensities were presented in multiple random density (mrd) units.

3. RESULTS AND DISCUSSION

Table 1 shows the U7.4Mo and U9.5Mo chemical compositions. The total impurities are approximately 2000 $mg.kg^{-1}$ among which the elements C, Al, Mn, and Fe stand out. The carbon

concentration is considered low and the impurities results are coherent compared to other works [11,12].

Table 1: Chemical composition of U-Mo alloys ($mg.kg^{-1}$ ± standard deviation). Values without standard deviation are below the detection limit of the equipment.

Element	U7.4Mo	U9.5Mo
N	9.75 ± 0.49	12.2 ± 2.5
C	260 ± 20	420 ± 20
Al	1335 ± 31	1000 ±42
B	43.1 ± 3.6	12.54 ± 0.01
Cr	< 1.00	< 1.27
Cd	< 2.08	< 2.64
Mn	253.2 ± 4.3	263.9 ±1.5
Fe	390.8 ± 17.8	393.0 ± 5.4
Co	< 0.028	< 0.028
Cu	5.85 ± 0.01	< 1.08
Zn	11.03 ± 0.98	15.9 ± 1.1
Ag	< 0.99	< 1.26
Zr	< 0.36	< 0.46
Ni	62.70 ± 0.01	77.4 ± 2.2
Gd	< 1.49	< 1.90
Si	< 0.008	< 0.008
V	< 0.006	< 0.006
Nb	< 0.002	< 0.002
Mo	73833 ± 80	95350 ± 650
W	< 0.041	< 0.041

The as-cast diffractograms (Figure 1) show that the alloys stabilized the γ-phase. The U9.5Mo x-ray diffraction peaks are dislocated to the right in comparison with U7.4Mo, this is due to the Mo atom is smaller than U atom and a decrease in lattice parameter occurs as the content of Mo is increased. This is confirmed by Rietveld refinement of the as-cast alloys. The lattice parameters obtained by Rietveld refinement are 3.412 Å and 3.429 Å for the U7.4Mo and U9.5Mo, respectively.

Figure 1: *As-cast U7.4Mo and U9.5Mo diffractograms.*

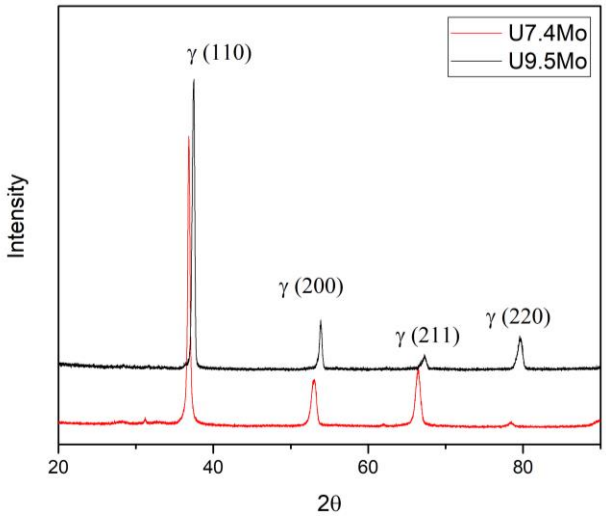

Figure 2 shows the as-cast U9.5Mo and U7.4Mo micrographs obtained by optical microscopy. Equiaxed grains with dendritic structure originated from solidification in the vacuum induction furnace were observed. The U7.4Mo alloy has a coarser dendritic structure than the U9.5Mo alloy.

Figure 2: *Micrographs of the as-cast U7.4Mo (a) and U9.5Mo (b).*

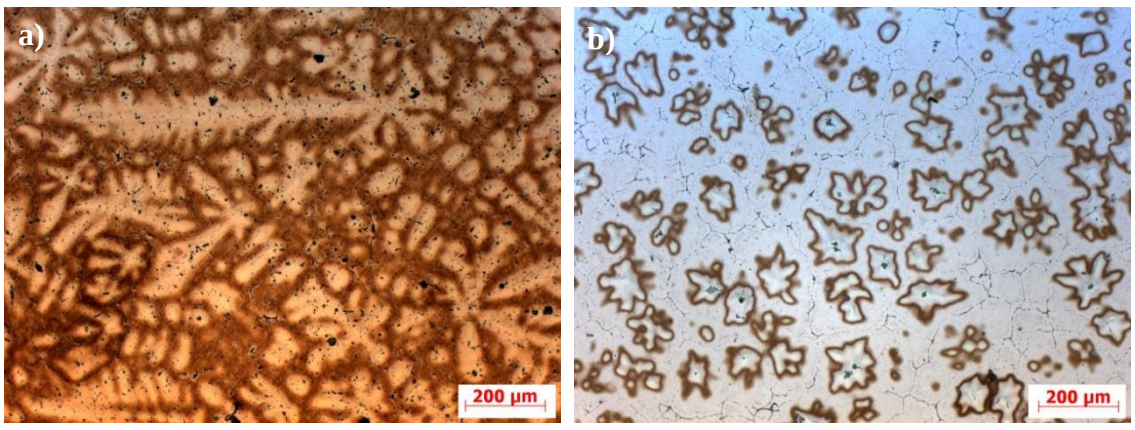

Molybdenum has higher corrosion resistance than the U and, as a consequence, the metallographic etching is more severe in regions with lower Mo content concluding that the solidification of the alloys starts in regions with higher molybdenum concentration and

microsegregation are presented in as-cast U-Mo alloys. This behavior is justified because the addition of molybdenum increases the melting point and therefore the regions with the highest molybdenum concentration solidify first [13]. Grains average sizes are 152.5 ± 28.8 μm and 76.1 ± 5.5 μm for the U7.4Mo and U9.5Mo as-cast alloys, respectively.

The contrast differences in backscattered electrons (BSE) images obtained by scanning electron microscope (Figure 3) suggest the microsegregation of the as-cast alloys [14]. It is noticed in the center of the dendritic grain darker contrast probably to a higher concentration of Mo. In micrographs by electron microscopy, it is also possible to observe the coarse dendritic structure of the U7.4Mo alloy.

Figure 3: *Micrographs obtained by backscattered electrons from the as-cast U7.4Mo (a) and U9.5Mo (b).*

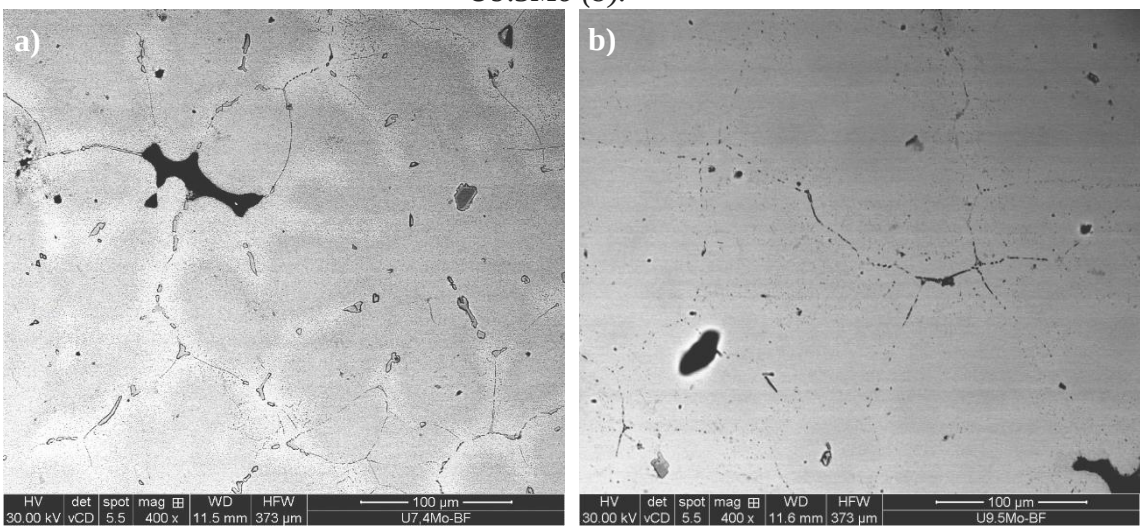

The results of the as-cast U-Mo alloys indicate the necessity for homogenization of the alloy. Microstructure region with low Mo content is more favorable for decomposition the γ-U from the eutectoid reaction UMo = U_2Mo + α-U [12] making an important factor for the production of monolithic nuclear fuels. Homogenized UMo alloys are necessary to obtain for decreasing phase transitions probability during the irradiation of these alloys [12,15].

Considering that the as-cast alloys U7.4Mo and U9.5Mo presented microsegregation, a homogenization treatment was performed. As in the as-cast samples, the gamma phase was found in homogenized U-Mo alloys. These results are seen in the x-ray diffractograms (Figure 4).

Another aspect observed in the diffractograms of the thermally treated U-Mo alloys is the width of the peak which is reduced indicating refinement of the alloy. The lattice parameters of homogenized alloys are 3.440 Å and 3.421 Å for the U7.4Mo and U9.5Mo, respectively. Comparing with the as-cast alloys the lattice parameters of the homogenized U-Mo alloys increase approximately 0.3%.

Figure 4: *Diffractograms of the U7.4Mo and U9.5Mo thermally treated alloy.*

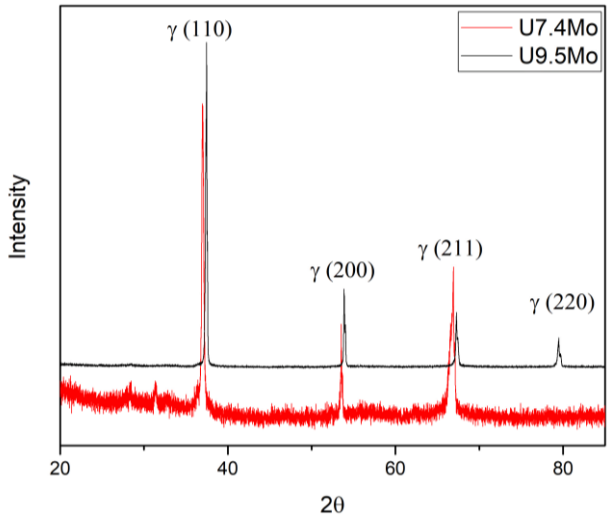

The microstructures of the thermally treated alloys are shown in Figure 5. As observed in these figures the dendrites in both alloys are consumed.

Figure 5: *Micrographs of the heat treated U7.4Mo (a) U9.5Mo (b).*

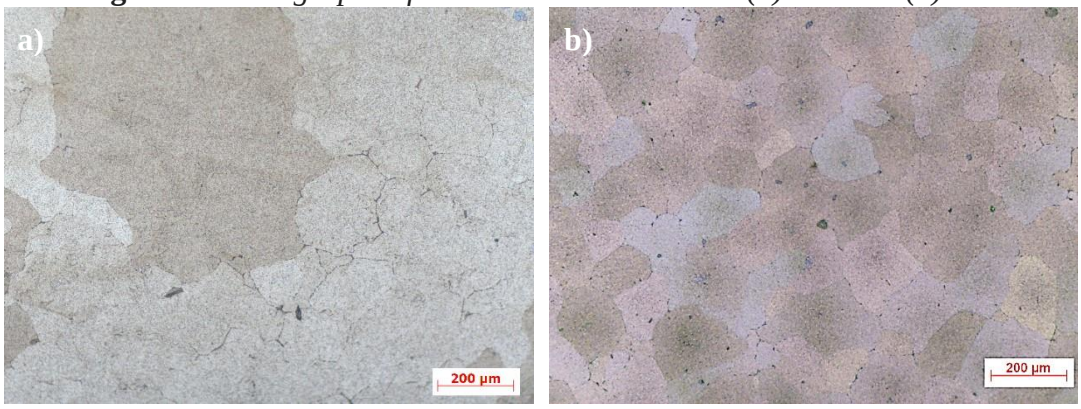

BSE images (Figure 6) show that the homogenization is obtained. The homogenization treatment diffuses Mo in the alloy. It can be observed in Figure 5 that equiaxed grains and the average grain size obtained were 174.5 ± 27.6 μm for U7.4Mo and 97.5 ± 4.5 μm for U9.5Mo. Comparing the mean grain size of as-cast with the homogenized alloys a growth of 14.4% for U7.4Mo and 28.1% for U9.5Mo. This percentage of growth difference can be explained in terms of the activation energy for grain growth. The U9.5Mo alloy has lower activation energy than the U7.4Mo alloy. The higher the activation energy for grain growth, the lower is the grain growth rate [16]. The grain size increasing of the homogenized samples did not change significantly compared to 1000°C U-Mo alloys homogenization treatment studies [14,17].

Figure 6: *Heat treated U7.4Mo (a) U9.5Mo (b) Electron backscattered micrographs.*

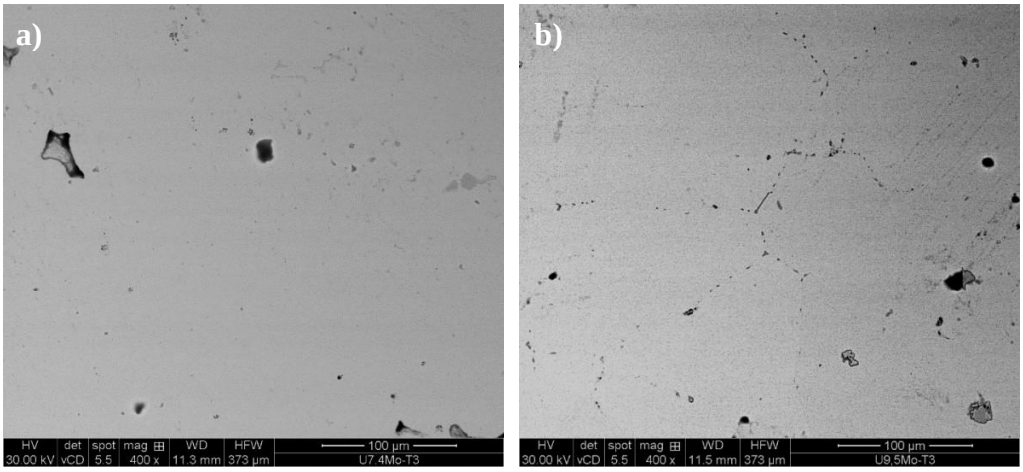

Figure 7 shows the ODF's φ_2 = 45° sections for U7.4Mo and U9.5Mo alloys deformed in 50%, 65%, and 80% thickness reduction. In general, it is noted that the alpha {hkl}[110], gamma (111)[uvw] and theta fibers (001)[uvw] are present in all deformation and its intensities vary with deformation. The position of these fibers in ODF φ_2 = 45° section is indicated in Figure 7b. Figure 8 shows the γ, α, and θ-fibers of hot rolled U-Mo alloys.

In 50% deformed alloys γ-fiber is strong in both alloys. The {111}<123> and (111)[011] texture components in U7.4Mo is stronger (11.2 mrd) than other γ-fiber components. The most intense γ-fiber component in U9.5Mo is (111)[011] (9.6 mrd). After rolling 65% thickness reduction, both

alloys show a strong homogeneous γ-fiber. By raising the deformation to 80% γ-fiber intensity decreases.

The α-fiber in hot rolled U-Mo alloys with 50% reduction is weak for U7.4Mo. In this reduction, the α-fiber in U9.5Mo is moderated at (112)[110] and strong at rotated cube (001)[110]. With 65% reduction, α-fiber slightly increases at (112)[110] in both alloys and the intensity of the rotated cube component is reduced in U9.5Mo. After hot rolling to 80% reduction, an intensification in the rotated cube orientation and the (112)[110] components were developed in U-Mo alloys.

With 50% reduction, θ-fiber is weak in U7.4Mo and strong in U9.5Mo. This fiber is weak in both alloys with 65% reduction and increases in the samples deformed at 80%. The rotated cube is the most intense θ-fiber texture component in 80% deformed U-Mo alloys.

Figure 7: *ODF's φ_2 = 45° sections of the U7.4Mo with 50 (a), 65 (c) and 80 (e)% reduction; U9.5Mo with 50 (b), 65 (d), and 80 (f)% reduction.*

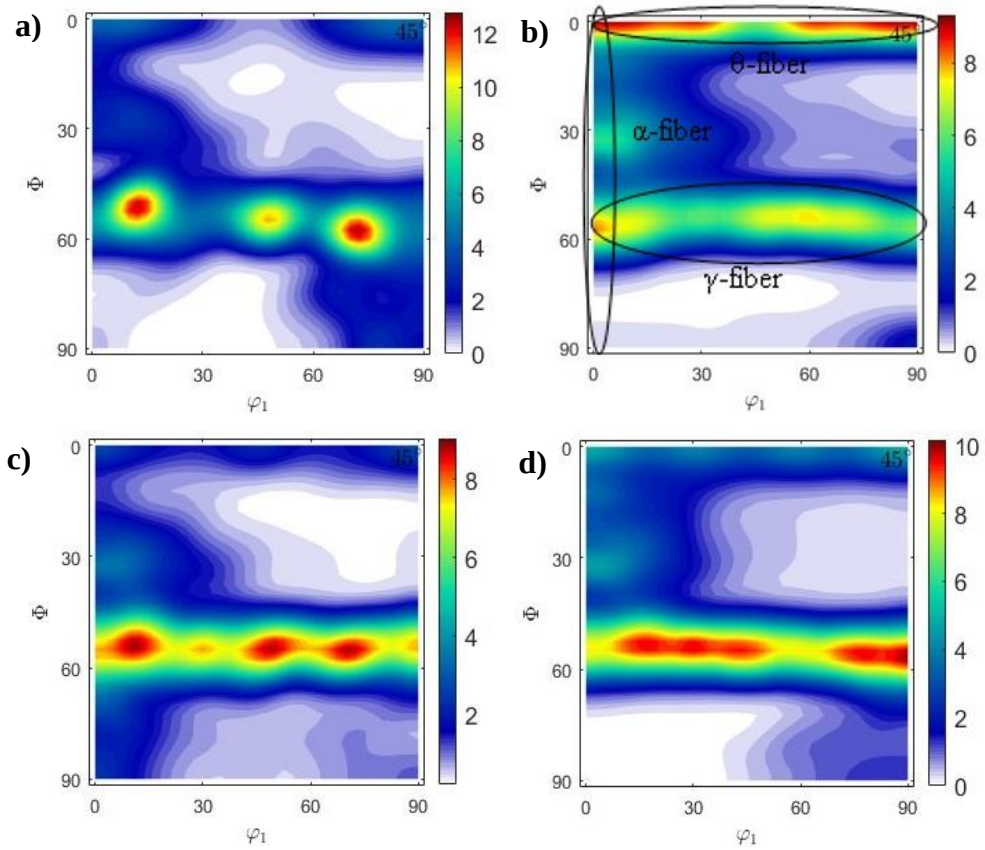

Continue on next page

Figure 7 (continued)

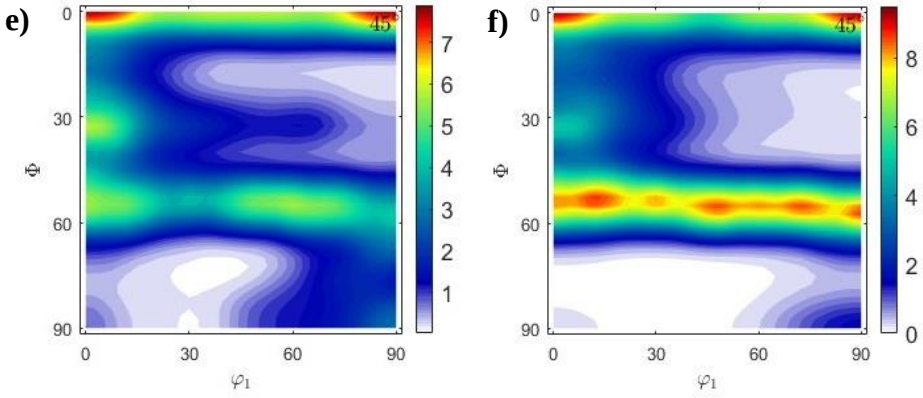

Figure 8: *γ (a,b), α (c, d) and θ (e, f) fibers of hot rolled U-Mo alloys.*

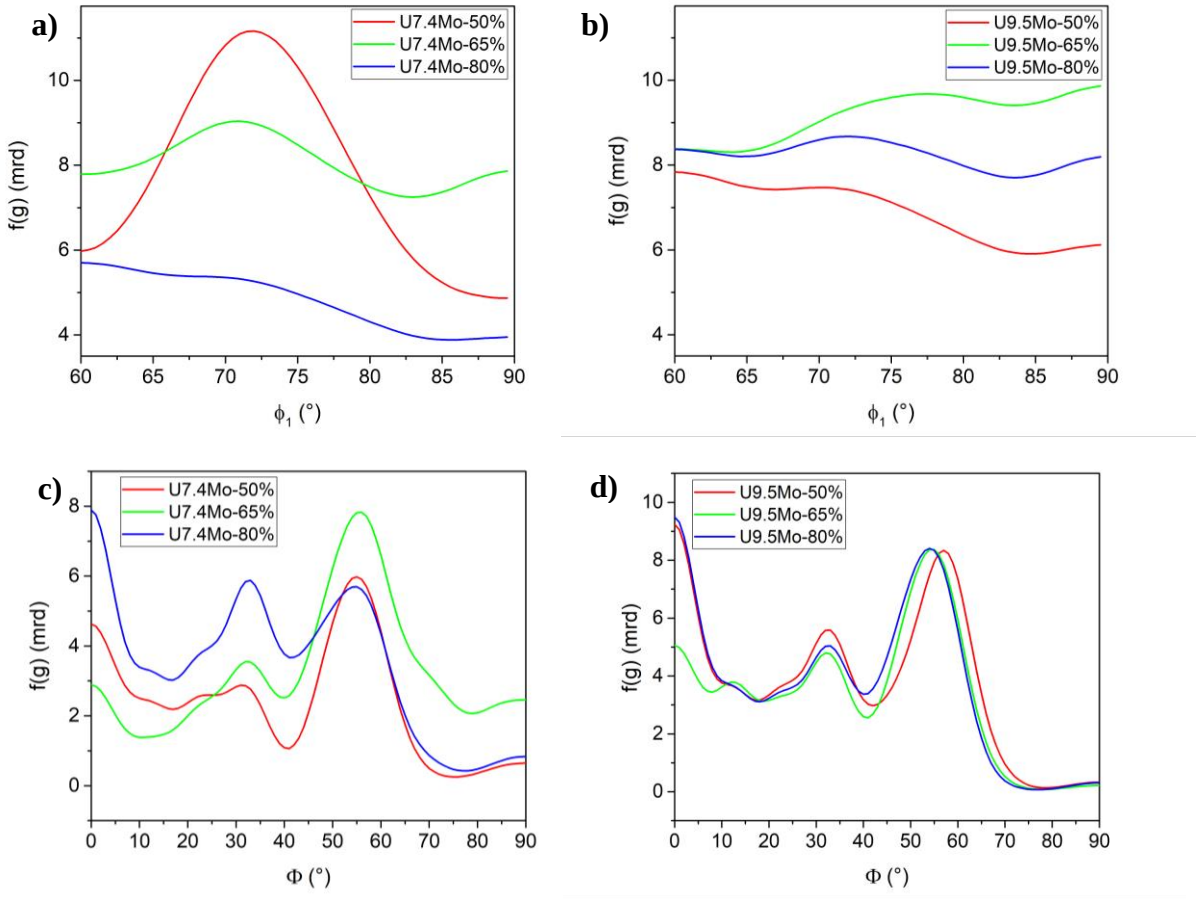

Continue on next page

Figure 8 (continued)

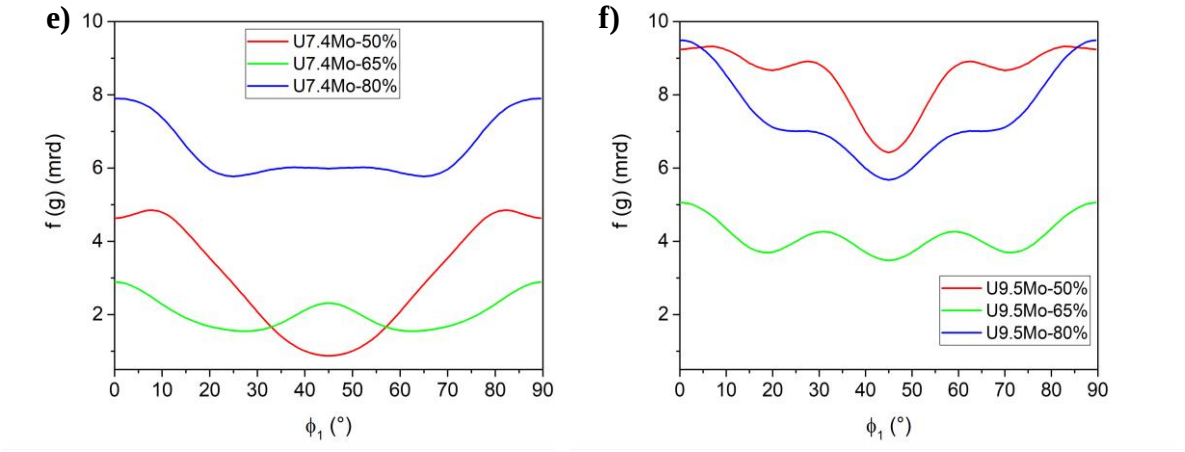

These textures fibers are commonly observed in other bcc materials [18-20]. In uranium alloys texture studies, similar results were observed in the cold rolled UNbZr alloy. Lopes et al. reported the presence of intense θ-fiber and moderated γ-fiber in U7.5Nb2.5Zr deformed at 80% [13].

The reduction intensity of gamma fiber components occasioned by increasing the thickness reduction was observed in cold rolled bcc steel by Kestens and Pirgazi [18]. It was observed in this work that the rising in the deformation from 83% to 90% the α-fiber component {112}<110> increases and γ-fiber decreases. At 99.9% deformation, a strong rotated cube component was observed [18].

The differences in texture between U7.4Mo and U9.5Mo could be caused by the initial grain size and stacking fault energy as a consequence of Mo constituent variation [21].

The alpha, gamma, and theta fiber textures found in the U-Mo alloys hot rolled with 80% reduction result to the isotropic properties of the materials. Monolithic fuels with isotropic properties are important to obtain due to the symmetrical swelling and thermal expansion behavior. Therefore, these properties contribute to the nuclear reactor stability [13].

4. CONCLUSION

The microstructure, texture results of homogenized and deformed U-Mo alloys give the following conclusions:

a. The as-cast alloys presented coarse dendritic structures, microsegregation, and the gamma phase.

b. The homogenization treatment consumed the dendrites and eliminated the microsegregation without significant grain growth.

c. The deformed uranium molybdenum alloys presented strong γ and θ fibers and moderated α fiber.

d. The evolution of texture fibers as the increasing deformation contributes to reducing the anisotropic properties of the material.

ACKNOWLEDGMENT

The authors would like to thank the Centro Tecnológico da Marinha em São Paulo, Centro Industrial Nuclear de ARAMAR and Instituto de Pesquisas Energéticas e Nucleares for the support in the development of this work.

REFERENCES

[1] PASQUALINI, E. E.; ROBINSON, A. B.; PORTER, D. L.; WACHS, D. M.; FINLAY, M. R. Fabrication and testing of U - 7Mo monolithic plate fuel with zircaloy cladding, **J. Nucl. Mater.**, v. 479, p. 402-410, 2016.

[2] WACHS, D. M. **RERTR fuel development and qualification plan**, Idaho Falls: Idaho National Laboratory, 2007. 65p.

[3] LOPES, D. A. **Interação entre precipitação e recristalização em liga de urânio contendo nióbio e zircônio (Mulberry alloy)**, São Paulo: Universidade de São Paulo, 2014. 176p.

[4] JOSHI, V. V.; NYBERG, E. A.; LAVENDER, C. A.; PAXTON, D.; GARMESTANI, H.; BURKES, D. E. Thermomechanical process optimization of U-10wt% Mo--Part 1: high-temperature compressive properties and microstructure, **J. Nucl. Mater.**, v. 465, p. 805-813, 2015.

[5] LISBOA, H.; MARIN, J.; BARRERA, M. Engineering of fuel plates on uranium-molybdenum monolithic: critical issues, **World J. Nucl. Sci. Technol.**, v. 5, p. 274-286, 2015.

[6] SURYAMAN, G. K.; WILDAN, M. W. Production of uranium − molybdenum alloy as a candidate for nuclear research reactor fuel, **Urania**, v. 24, n. 3, p. 135-142, 2018.

[7] CLARK, C. R.; KNIGHTON, G. C.; MEYER, M. K.; HOFMAN, G. L. Monolithic fuel plate development at argonne national laboratory, In: **INTERNATIONAL MEETING ON REDUCED ENRICHMENT FOR RESEARCH AND TEST REACTORS**, 2003, Chicago. Annals... Chicago: Argonne National Laboratory, 2003.

[8] PEREZ, E.; YAO, B.; KEISER, D. D.; SOHN, Y. H. Microstructural analysis of as-processed U-10 wt.%Mo monolithic fuel plate in AA6061 matrix with Zr diffusion barrier, **J. Nucl. Mater.**, v. 402, n. 1, p. 8-14, 2010.

[9] TOBY, B. H. EXPGUI, a graphical user interface for GSAS, **J. Appl. Crystallogr.**, v. 34, n. 2, p. 210-213, 2001.

[10] HIELSCHER, R.; SCHAEBEN, H. A novel pole figure inversion method : specification of the MTEX algorithm, **J. Appl. Cryst.**, v. 41, p. 1024–1037, 2008.

[11] DE OLIVEIRA, F. B. V.; DE CARVALHO, E. F. U.; RIELLA, H. G. Fabrication results of gamma uranium-molybdenum alloys fuels, In: **INTERNATIONAL NUCLEAR ATLANTIC CONFERENCE**, 2009, Rio de Janeiro. Annals… Rio de Janeiro, Comissão Nacional de Energia Nuclear, 2009.

[12] CLARKE, A. J.; CLARKE, K. D.; MCCABE, R. J.; NECKER, C. T.; PAPIN, P. A.; FIELD, R. D.; KELLY, A. M.; TUCKER, T. J.; FORSYTH, R. T.; DICKERSON, P. O.; FOLEY, J. C.; SWENSON, H.; AIKIN, R. M.; DOMBROWSKI, D. E. Microstructural evolution of a uranium-10 wt.% molybdenum alloy for nuclear reactor fuels, **J. Nucl. Mater.**, v. 465, p. 784-792, 2015.

[13] LOPES, D. A.; RESTIVO, T. A. G.; N. B. DE LIMA, PADILHA, A. F. Gamma-phase homogenization and texture in U–7.5Nb–2.5Zr (Mulberry) alloy, **J. Nucl. Mater.**, v. 449, p. 23-30, 2014.

[14] JOSHI, V. V.; NYBERG, E. A.; LAVENDER, C. A.; PAXTON, D.; BURKES, D. E. Thermomechanical process optimization of U-10wt% Mo – Part 2: The effect of

homogenization on the mechanical properties and microstructure, **J. Nucl. Mater.**, v. 465, p. 710-718, 2015.

[15] JANA, S.; SCHEMER-KORHN, A.; OVERMAN, N.; SWEET, L.; KAUTZ, E.; LAVENDER, C.; JOSHI, V. **Eutectoid Transformation in U10Mo Alloy : Effect of Deformation History and Homogenization Heat Treatment**, Richland: Pacific Northwest National Laboratory, 2019. 34p.

[16] FRAZIER, W. E.; HU, S.; OVERMAN, N.; LAVENDER, C.; JOSHI, V. V. Short communication on Kinetics of grain growth and particle pinning in U-10 wt.% Mo, **J. Nucl. Mater.**, v. 498, p. 254-258, 2018.

[17] NEOGY, S.; SAIFY, M. T.; JHA, S. K.; SRIVASTAVA, D.; HUSSAIN, M. M.; DEY, G. K.; SINGH, R. P. Microstructural study of gamma phase stability in U-9 wt.% Mo alloy, **J. Nucl. Mater.**, v. 422, n. 1-3, p. 77-85, 2012.

[18] KESTENS, L. A. I.; PIRGAZI, H. Texture formation in metal alloys with cubic crystal structures, **Mater. Sci. Technol.**, v. 32, n. 13, p. 1303-1315, 2016.

[19] LOBANOV, M. L.; DANILOV, S. V.; PASTUKHOV, V. I.; AVERIN, S. A.; KHRUNYK, Y. Y.; POPOV, A. A. The crystallographic relationship of molybdenum textures after hot rolling and recrystallization, **Mater. Des.**, v. 109, p. 251-255, 2016.

[20] ZHANG, Z.; CHEN, D.; ZHAO, H.; LIU, S. A comparative study of clock rolling and unidirectional rolling on deformation/recrystallization microstructure and texture of high purity tantalum plates, **Int. J. Refract. Met. Hard Mater.**, v. 41, p. 453-460, 2013.

[21] DILLAMORE, I. L.; ROBERTS, W. T. Rolling textures in f.c.c. and b.c.c. metals, **Acta Metall.**, v. 12, n. 3, p. 281-293, 1964.